Supporting Information

Männik et al. 10.1073/pnas.0907542106

SI Text

Measurements of Bacterial Diameters Using Fluorescent Images. For the measurement of bacterial diameters, we acquire a stack of images of bacteria between two coverslips by changing the focal plane of the 100× objective in 0.1-μm steps. We select the image where bacteria attached to the cover-slide are in focus and from this image extract intensity line profiles perpendicular to the long axes of individual bacteria. From the smoothed line profiles, we find two inflection points of the profile (points where the second derivative by coordinate along the axes of the profile becomes zero) which approximately correspond to the outer edges of bacterium along its diameter (Fig. S6). For a more accurate estimate, we have modeled the intensity profiles of bacteria and found that the inflection-point method underestimates the diameter of bacteria by 80 nm for the range of diameters of *E. coli* and *B. subtilis* bacteria (see section *Relation Between Inflection Point Estimate and Bacterial Diameter* below for details). Because GFP only fills the cytoplasmic space of the bacterium, a further correction is needed to take into account the extent of the outer membrane, cell-wall, periplasmic space, and inner membrane. For *E. coli*, this amounts 40 nm (1), and *B. subtilis* 125 nm (2). Adding these two correction factors to the inflection point estimate, we obtain the distributions shown in Fig. 4.

Relation Between Inflection Point Estimate and Bacterial Diameter. A simple estimation based on the distance between the inflection points underestimates the diameter of the cytosolic space of the bacterium. This method would yield the exact result if the cross-section of the bacterium was a rectangle but in reality the shape is close to a circle. To find the correction we have carried out modeling of intensity profiles of the bacterium. Intensity profiles of rod-shaped bacteria such as *E. coli* or *B. subtilis* can be calculated by convolution of the point-spread function (PSF) of the microscope over the cross-sectional area of the bacteria. For *E. coli* and *B. subtilis*, the cross-section is in a good approximation a circle.

The PSF of the microscope can be experimentally determined by measuring intensity profiles of objects much smaller than the resolution of the microscope. The PSF of the microscope can also be calculated using the known numerical aperture of the microscope and the wavelength of the emitted light. We have used both approaches and have found essentially identical results. For the experimentally measured PSF, we have used EviTag T2-MP CdSe core/shell quantum dots (Evident Technologies) which have an emission maximum close to the emission maximum of GFP. To account for the fact that not all points of the bacterium are simultaneously in focus, the PSF of the quantum dot point source can be determined by scanning the focal plane of the microscope, Fig. S7. The variation of the PSF by defocusing the microscope has, however, only a small effect on the resulting shape of the intensity profile. Similarly, a slight defocusing of the microscope ($\pm$0.3 μm) has a negligible effect on the location of the inflection points of the bacterial intensity profile.

One can use these experimentally determined PSFs to carry out a numerical convolution (Fig. S8). From these intensity profiles, the relationship between the bacterial diameter and the separation between the inflection points can be found (Fig. S9). Fitting a line to the data in Fig. S9 yields $D_{in} = W_{infl}+0.08$ μm. This relationship becomes valid when D is bigger than $\approx$0.4 μm. The latter value sets approximately the lower limit where bacterial diameters can be reliably extracted using our measurement setup. Thus, for $D_{in}>0.4$ μm, the inflection point can be used to estimate the true diameter of the bacterial inner membrane by adding a constant factor of 80 nm.

In summary, for the diameter of the outer membrane of *E. coli* we obtain $D = W_{infl}+0.12$ μm taking into account also the width of periplasmic space. Similarly, for the diameter of the outer membrane of *B. subtilis,* we obtain $D = W_{infl}+0.20$ μm. These relations were used to deduce the bacterial diameter, Fig. S10.

1. Matias VRF, Al-Amoudi A, Dubochet J, Beveridge TJ (2003) Cryo-transmission electron microscopy of frozen-hydrated sections of Escherichia coli and Pseudomonas aeruginosa. *J Bacteriol* 185:6112–6118.

2. Matias VRF, Beveridge TJ (2005) Cryo-electron microscopy reveals native polymeric cell wall structure in *Bacillus subtilis* 168 and the existance of a periplasmic space. *Mol Microbiol* 56:240–251.

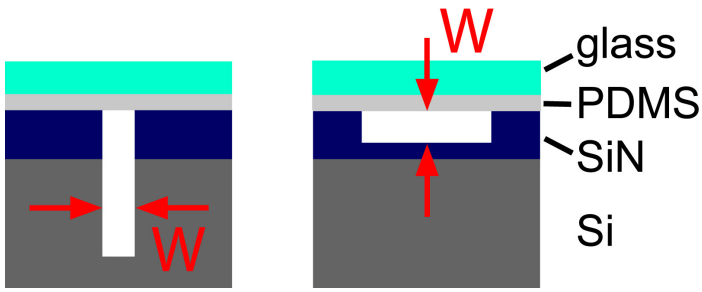

Fig. S1. Schematic cross-sectional view of the two types of channels used in this work. *Left*: vertical channels (down to 0.4-μm width) were etched deep and narrow into silicon. *Right*: horizontal shallow channels (with widths $<$0.4 μm) etched into a silicon nitride layer on the top of the silicon. Widths (*W*) for both types of channels are defined as indicated on the schematic.

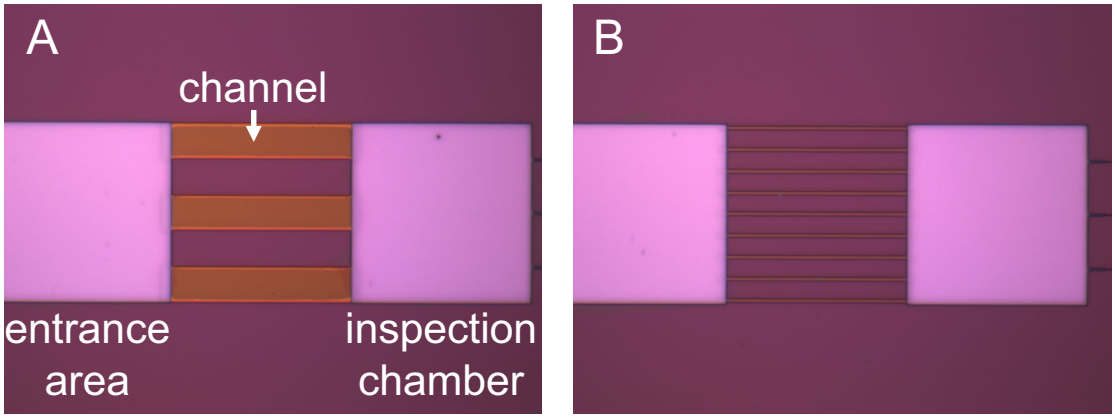

Fig. S2. Layout used in the chips with horizontal channels. The lateral dimensions of the channels vary from 10 μm (*A*) to 1 μm (*B*). Bacteria come to the entrance area, pass through the horizontal channels and then reach the inspection chamber where their transformation back to regular phenotype can be observed.

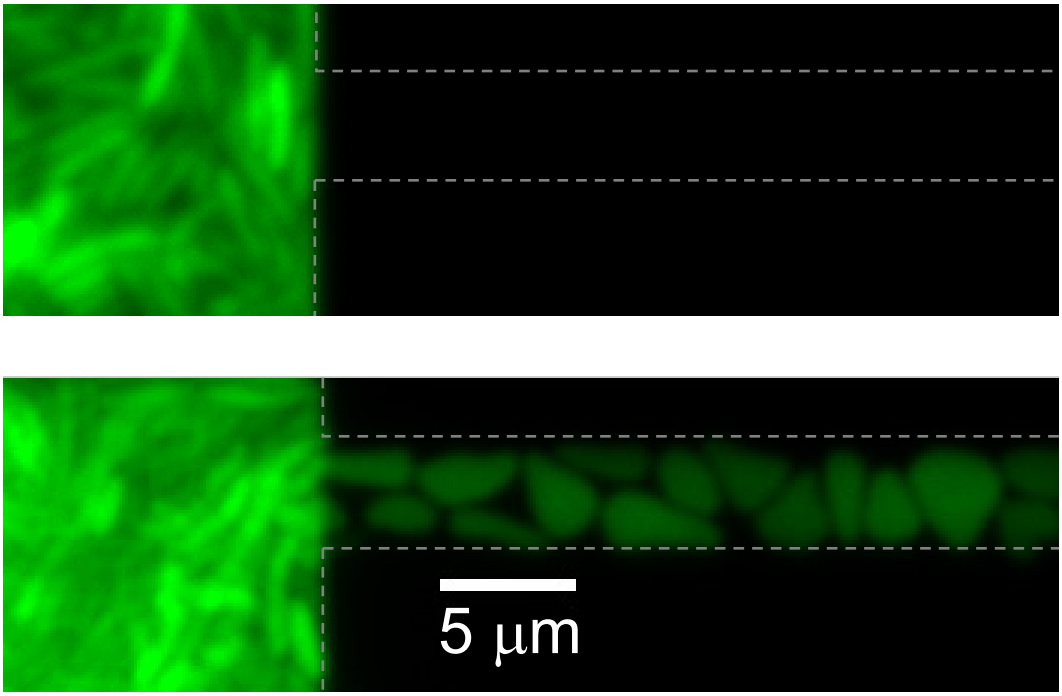

Fig. S3. Fluorescence images of *E. coli* bacteria before *(Top)* and after (*Bottom*) entering into horizontal channel of 0.3-μm width. The same channel is shown also in Fig. 5*A* (main text) at higher contrast and lower magnification. Using these image settings, it can be seen that the morphology of bacteria in the chamber area is regular rod-shape. Dashed lines mark approximately the borders of the chambers and channels. The scale bar is the same for both images.

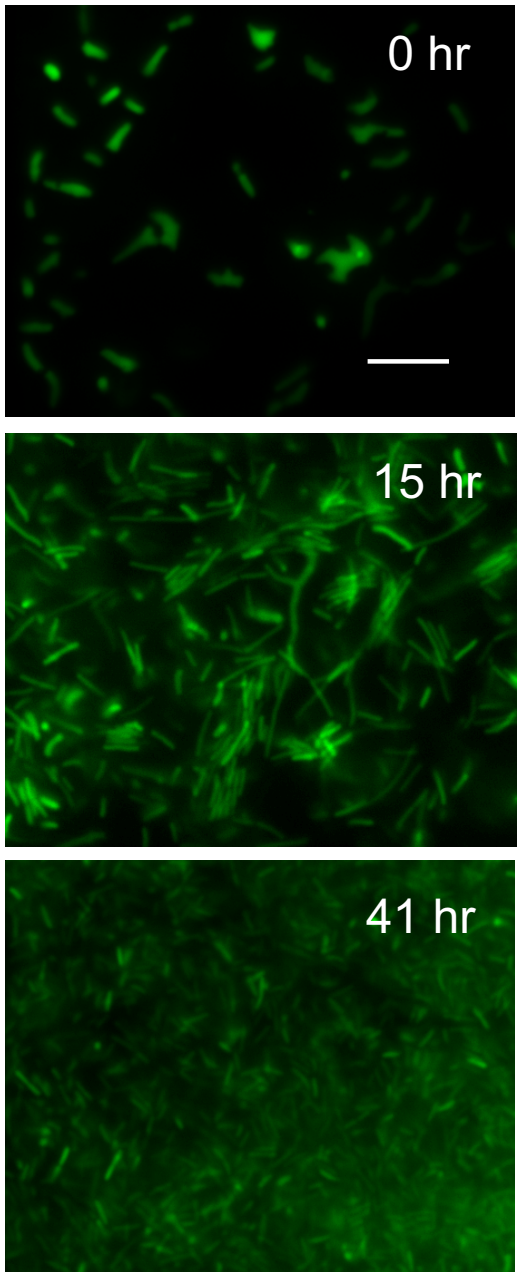

Fig. S4. Reversal of *E. coli* from aberrant to regular shapes. Fluorescence images of bacteria in a chamber which has been populated through a 0.7-μm wide channel. A transition from aberrantly shaped bacteria to a population of regular rod-shaped bacteria can be seen during a 41-h period. During this transition, bacteria also recover their motility. (Scale bar, 10 μm.)

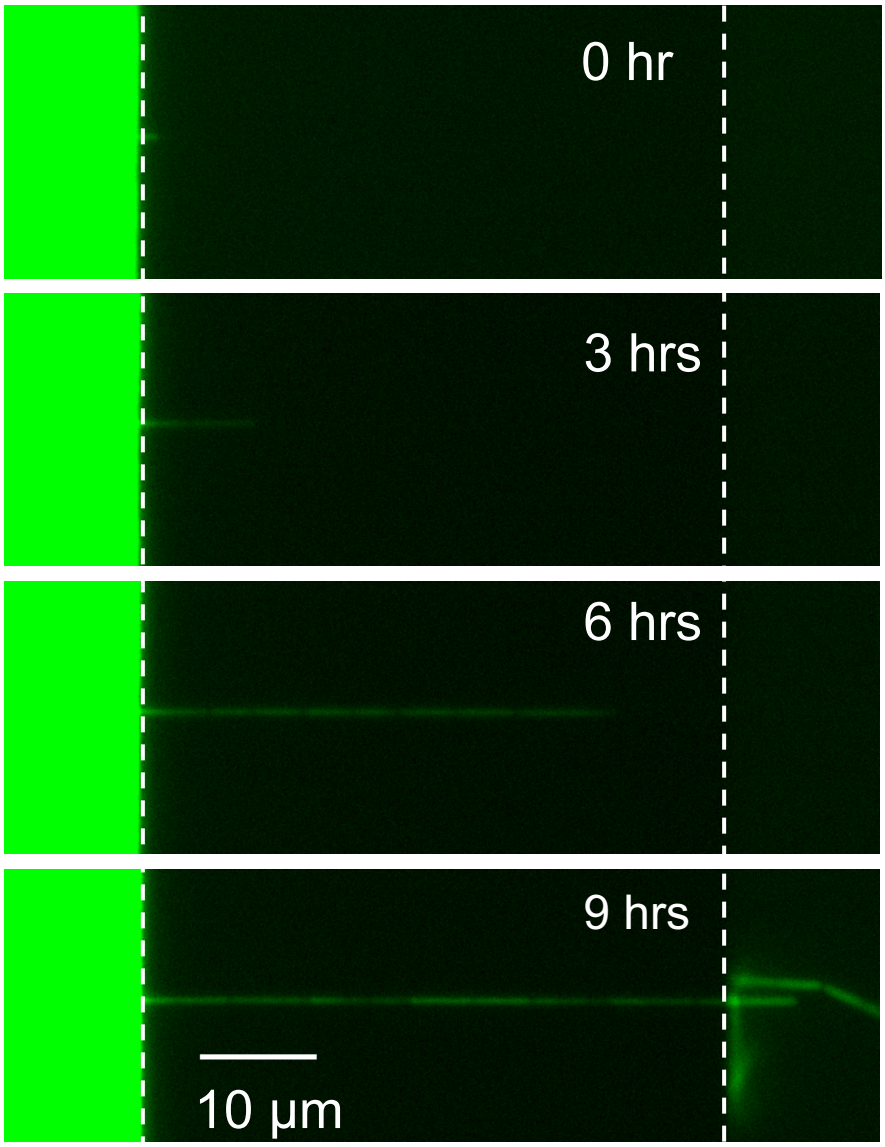

Fig. S5. Time-lapse fluorescent images of growth of *B. subtilis* P_{abr}-gfp cells through a 0.75-μm wide channel. Dashed lines mark the boundaries of the chambers.

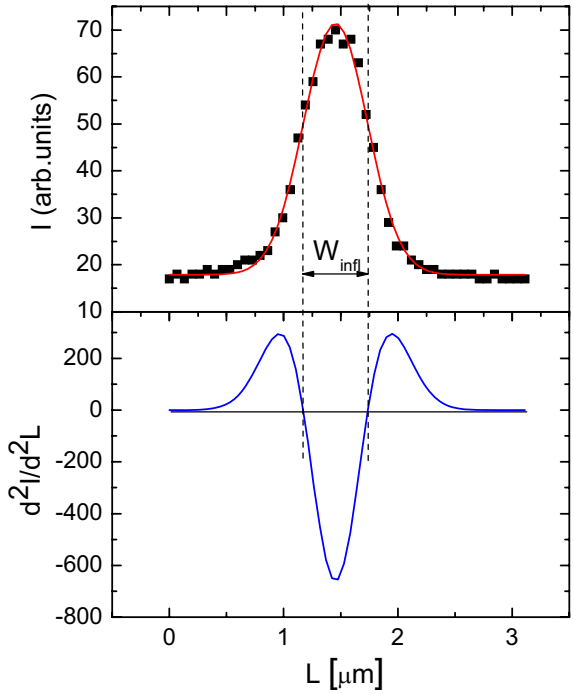

Fig. S6. ***Top***: Typical intensity profile of the GFP luminescence of an *E. coli* RP437 bacterium, measured perpendicular to bacterial long axis. The solid line represents the smooth interpolation curve for the data (in present case a Gaussian). ***Bottom***: The second derivative of the smoothed profile. Inflection points correspond to zero crossings of the second derivative.

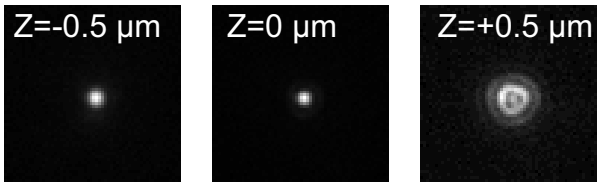

Fig. S7. PSF of our Olympus IX81 inverted microscope with a 100× NA = 1.4 oil immersion objective for three different positions of the focal plane. Intensities of each image are scaled separately to make details of the PSF visible. Full width at the half maximum of the narrowest PSF (*Middle* image) is 0.22 μm.

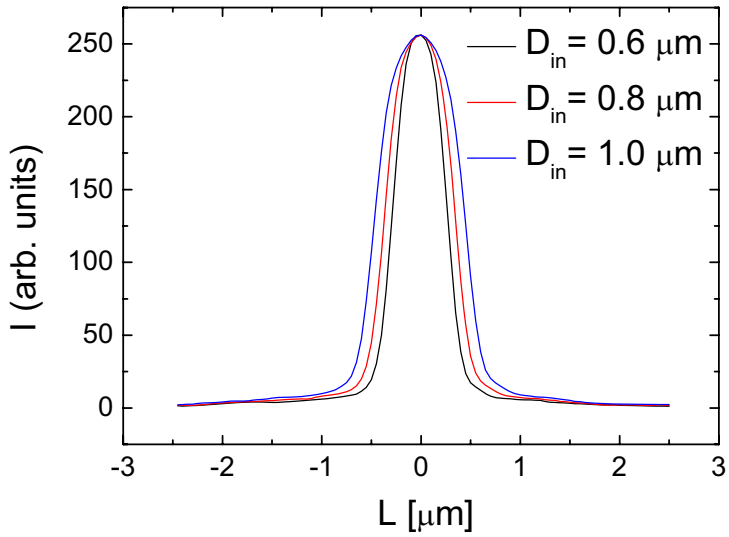

Fig. S8. Intensity profiles calculated for three different bacterial diameters (0.6, 0.8, and 1.0 μm) using the experimentally determined PSF of Fig. S7.

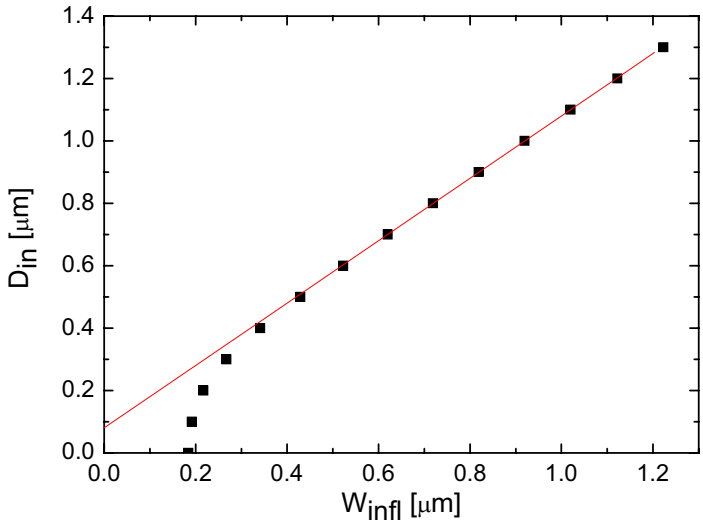

Fig. S9. Diameter defined by the inner membrane of bacterium vs. distance between inflection points. Squares are results of calculations. The solid line represents a linear fit to the calculated points for $D_{in} \geq 0.4$ μm.

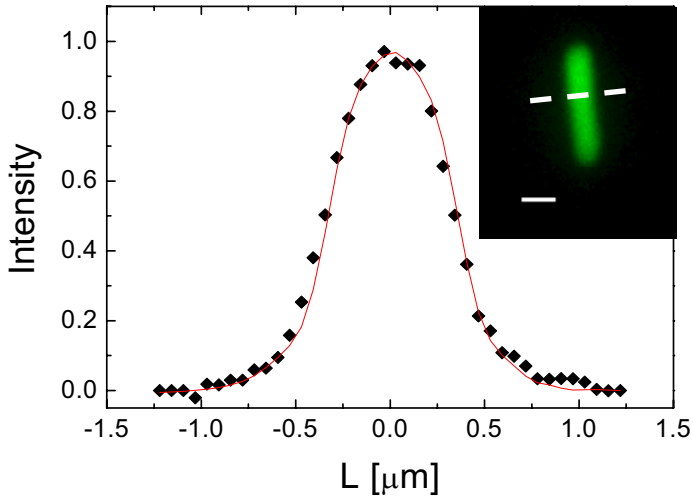

Fig. S10. Fluorescence intensity profile of the *E. coli* bacterium shown in the inset of the figure. The solid line represents the calculation of the intensity profile where D_{in} is taken as $W_{infl} + 0.08$ μm. Inflection points for W_{infl} are determined as described above. The scale bar in the *inset* is 1 μm.

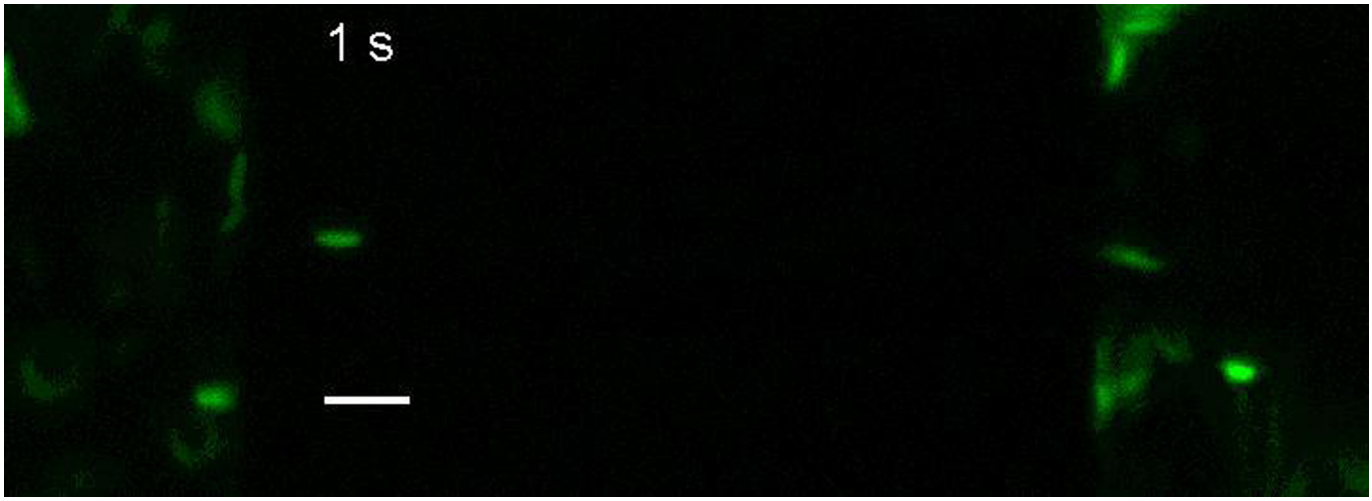

Movie S1. Bacterial motility in channel. Motility of GFP-labeled *E. coli* imaged in 1.3 μm wide silicon channel with the 60$\times$ objective in epifluorescence microscope. Bacterial movement in both directions in the channel can be seen as well as a tumble of a bacterium moving from right to left. The bacteria exiting the channel can also traced in the chambers. (Scale bar, 5 μm.)

Movie S1 (AVI)

Movie S2. Growth of *E. coli* in narrow silicon channel. Growth of GFP-labeled *E. coli* has been recorded in 0.8-μm silicon channel with the 60$\times$ objective in epifluorescence microscope. Images have been acquired at every 15 min and played back at frame rate 5 frames/s. (Scale bar, 10 μm.)

Movie S2 (AVI)

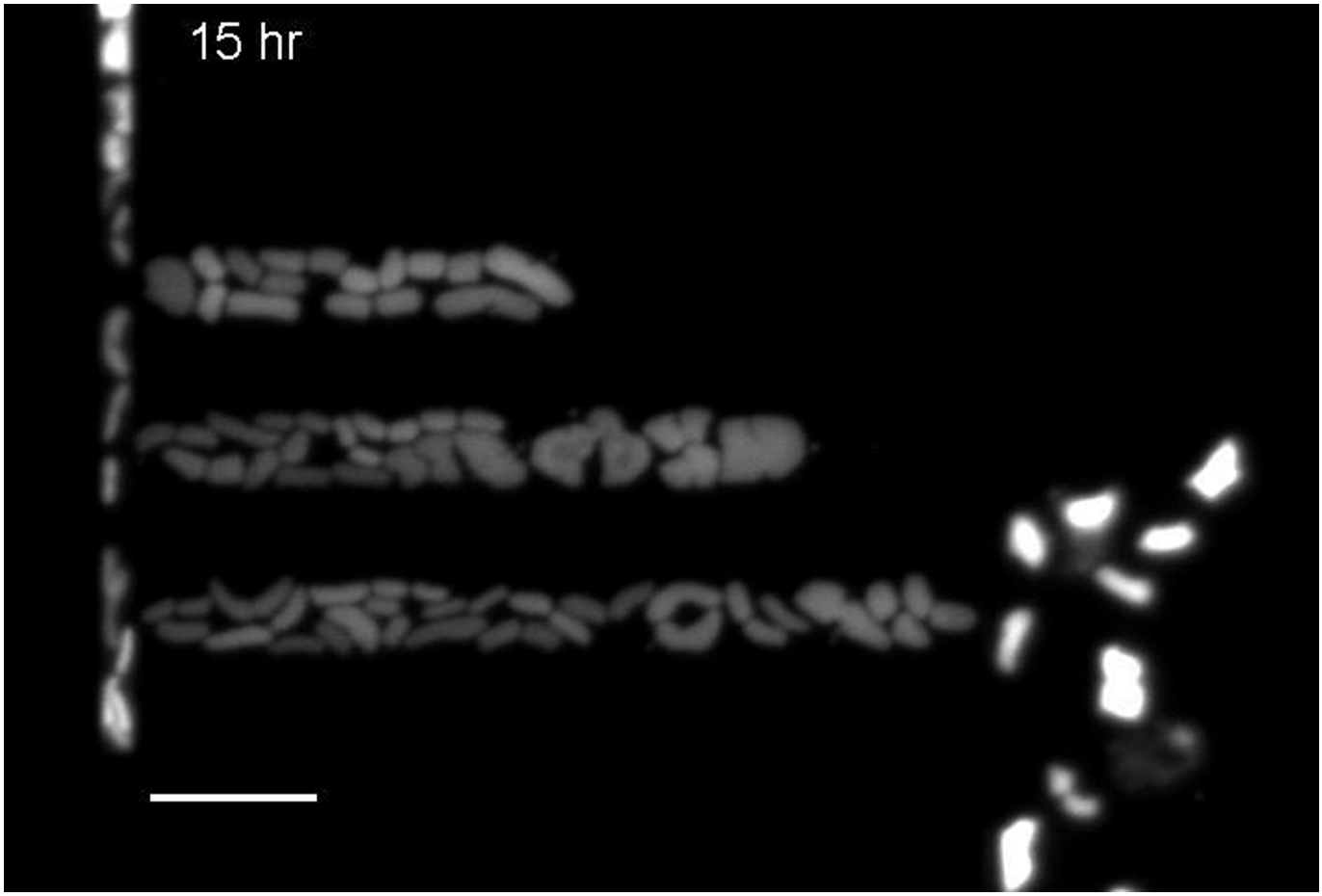

Movie S3. Formation of aberrantly shaped bacteria. Morphological changes in *E. coli* has been recorded in 0.3 μm deep PDMS-silicon channel with the 60× objective in epifluorescence microscope. (Scale bar, 10 μm.)

Movie S3 (AVI)

Movie S4. Formation of aberrantly shaped bacteria. Morphological changes in *E. coli* has been recorded in 0.3 μm deep PDMS-silicon channel with the 60× objective in epifluorescence microscope. (Scale bar, 10 μm.)

Movie S4 (AVI)

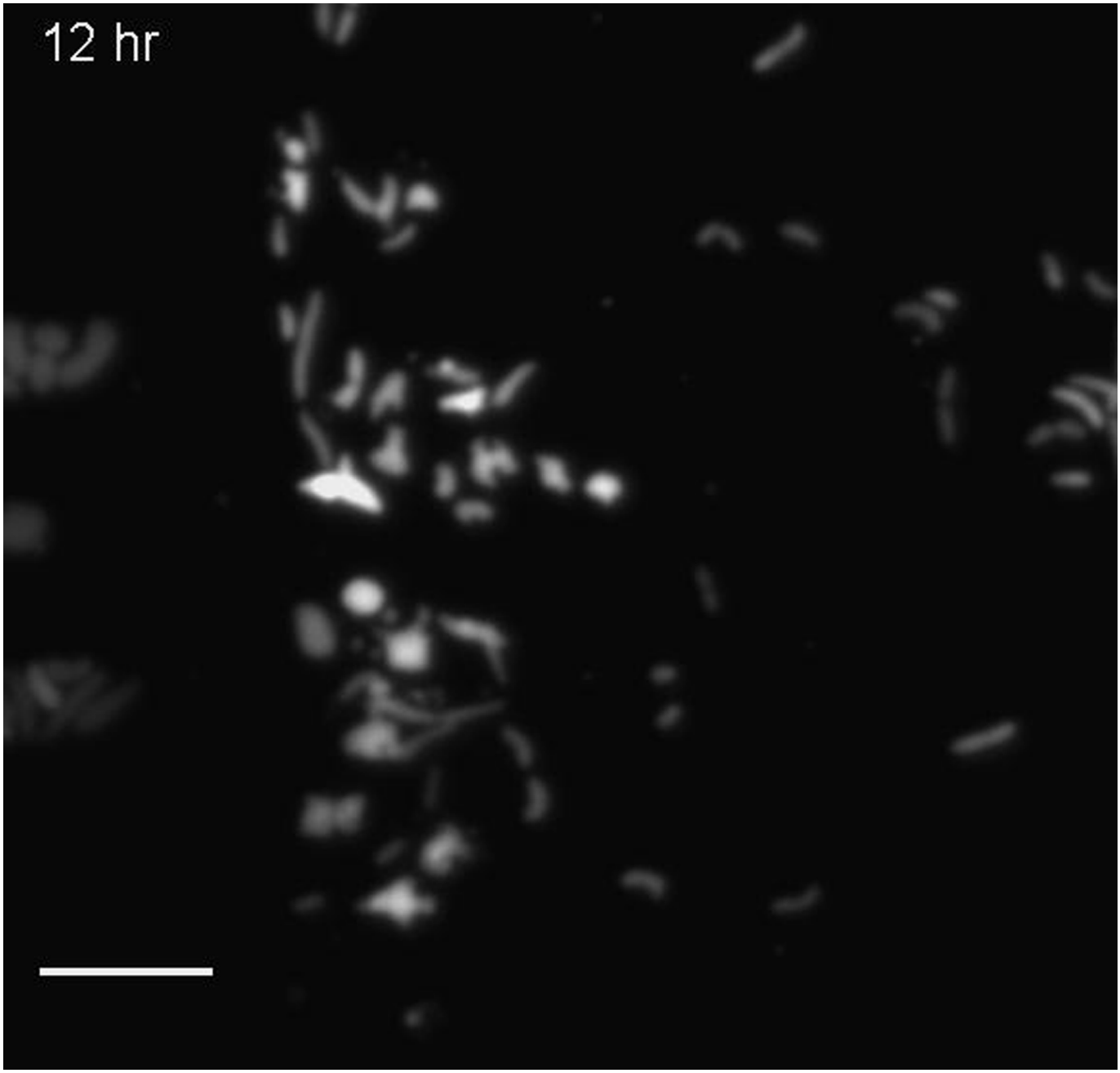

Movie S5. Reversion of aberrantly shaped bacteria back to regular rod-shaped form. *E. coli* in 0.3-μm deep PDMS-silicon channel (left) and in 1.8-μm deep chamber (right) have been recorded with the 60$\times$ objective in epifluorescence microscope. (Scale bar, 10 μm.)

Movie S5 (AVI)

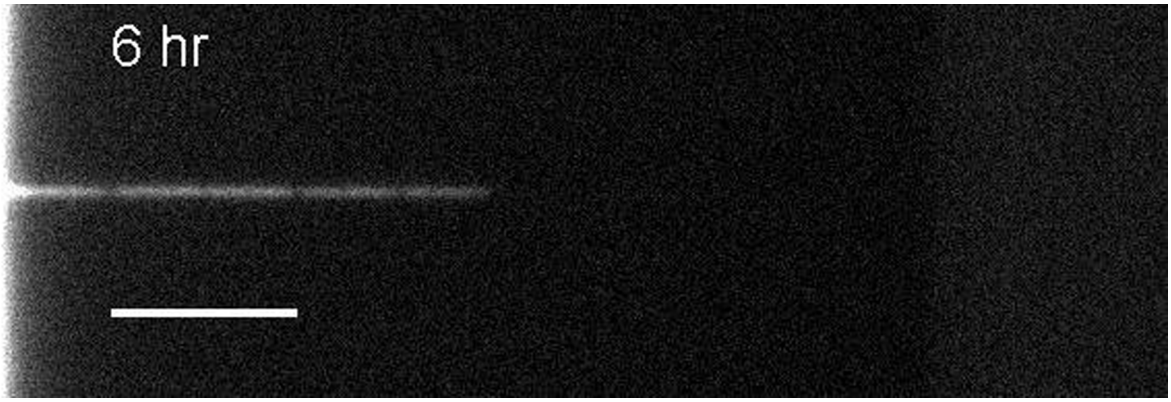

Movie S6. Growth of *B. subtilis* in narrow silicon channel. Growth of GFP-labeled *B. subtilis* has been recorded in 0.75-μm wide silicon channel with the 60$\times$ objective in epifluorescence microscope. (Scale bar, 10 μm.)

Movie S6 (AVI)